CRYSTAL GROWTH & DESIGN

pubs.acs.org/crystal

Article

Large Single Crystals of $V_{1-x}Mo_xO_2$ from a Two-Step Chemical Vapor Transport Synthesis

Matthew A. Davenport, Matthew P. Confer, Tyra C. Douglas, Top B. Rawot Chhetri, and Jared M. Allred*

Cite This: *Cryst. Growth Des.* 2020, 20, 3635−3640

Read Online

ACCESS | Metrics & More | Article Recommendations | Supporting Information

ABSTRACT: Single crystals of molybdenum doped VO_2 with the formula $V_{1-x}Mo_xO_2$ have been successfully synthesized with molybdenum compositions up to $x = 0.60$. These crystals were obtained using a novel, two-step chemical vapor transport (CVT) synthesis. The first CVT reaction uses a stoichiometric amount of VO_2, V_2O_3, MoO_2, and MoO_3 with $MoCl_3$ as a transport agent to produce a largely polycrystalline, single phase $V_{1-x}Mo_xO_2$ product. This product can then be pulverized and used in a second CVT reaction with $TeCl_4$ as a transport agent to produce large single crystals. This two-step synthetic method results in larger single crystals with a higher degree of compositional control compared to any single step CVT syntheses attempted, as well as allowing for an increase in dopant range compared to what had previously been achieved for this dopant system. Crystals obtained from this synthetic method are ideal for physical property measurements and diffuse scattering experiments which require large samples to be able to properly mount the samples and obtain useful data.

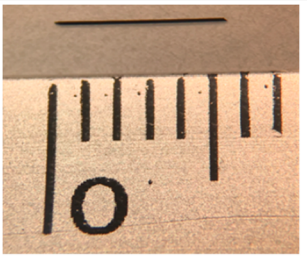

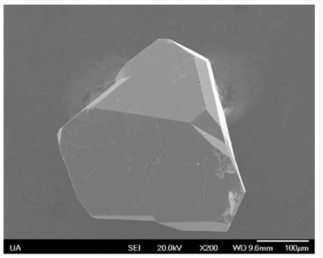

INTRODUCTION

Vanadium dioxide is one of several known materials with a metal-to-insulator transition (MIT) occurring under certain conditions, usually as a function of temperature. This MIT, first discovered in 1959, occurs at 340 K and is signified by a large change in resistance up to 5 orders of magnitude, as well as a structural phase transition (SPT) from a low-temperature insulating monoclinic phase (M1) to a high-temperature metallic tetragonal phase (R).[1,2] Although the MIT in VO_2 was first observed six decades ago, the mechanism behind this transition remains in question. There are two main mechanisms generally considered to play a role in the transition, the Mott−Hubbard mechanism, which is driven by electron−electron correlations, resulting in antiferromagnetic ordering, and the Peierls mechanism, which is driven by electron−phonon correlations, resulting in bond formation.[3,4] While the transition is often considered to be caused by a combination of the two mechanisms, determining which is the driving force behind the change in resistivity remains a topic of debate in VO_2 research.[5−7]

Substitution of VO_2 with other transition metals can contribute to this debate by determining how changes in the MIT and SPT are related to the two mechanisms. Transition metal substitution can either change the bonding orbitals, the number of valence electrons, or both at the same time, meaning the mechanism is likely altered in the process. This means that doping other metals can have a significant impact on the temperature of the MIT with dopants, such as tungsten causing a suppression of the MIT temperature between 23 and 26 K per percent dopant.[8−10] Doping can also change the structure, as it is with the emergence of a separate monoclinic structural phase (M2) when substituting in chromium, titanium, and aluminum.[11−13]

In previous work done on the $V_{1-x}Mo_xO_2$ dopant system, it has been shown that as the composition of molybdenum increases, the insulating monoclinic phase becomes more metallic while both the magnitude of the change in resistance and the transition temperature decrease until the MIT completely disappears around 20% molybdenum composition even though the transition should remain well above 0 K at this composition.[9] Additionally, this previous work found evidence of a monoclinic ordered phase from the electron diffraction pattern for $V_{0.5}Mo_{0.5}O_2$, which was the highest molybdenum composition obtained; however, evidence of this phase was not seen in synchrotron powder X-ray diffraction data.[9] To determine the structural phase of the superlattice present in $V_{0.5}Mo_{0.5}O_2$, as well as, to better determine why the MIT disappears around 20% molybdenum concentration, we have determined an appropriate synthetic method to obtain large

Received: September 30, 2019
Revised: April 22, 2020
Published: April 22, 2020

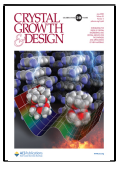

Table 1. Results of CVT Synthesis[a]

starting materials	ratio V: Mo: O	transport agent	$V_{1-x}Mo_xO_2$ x =	byproducts
VO_2, V_2O_3, MoO_3	0.80:0.20:2.2	$TeCl_4$	0.418(11)[a]	$Mo_4V_9O_{25}$[a]
VO_2, V_2O_3, MoO_3	0.80:0.20:2.1	$TeCl_4$	0.159(7)[a]	$Mo_{0.9}V_{1.1}O_5$[a]
VO_2, V_2O_3, MoO_3	0.80:0.20:2.0	$TeCl_4$	0.163(7)[a]	$TeMo_5O_{16}$[ab]
VO_2, V_2O_3, MoO_3	0.80:0.20:1.9	$TeCl_4$	0.157(7)[a]	V_4O_7[a]
VO_2, V_2O_3, MoO_3	0.80:0.20:1.2	$TeCl_4$	0.045(6)[a]	V_3O_5[a]
VO_2, V_2O_3, MoO_3	0.67:0.33:2	$TeCl_4$	0.294(9)[a]	$TeMo_5O_{16}$[ab], $TeMo_4O_{13}$[a]
VO_2, V_2O_3, MoO_3	0.50:0.50:2.25	$TeCl_4$	N/A	$TeMo_5O_{16}$[ab], MoO_3[b]
V_2O_3, MoO_3, MoO_2	0.60:0.40:2	$TeCl_4$	0.187(7)[b]	MoO_2[a]
V_2O_3, MoO_3, MoO_2	0.50:0.50:2	$TeCl_4$	0.242(8)[b]	$TeMo_5O_{16}$[ab], $(Mo_{1.83}V_{1.17})Te_{0.88}O_{9.25}$[b]
VO_2, V_2O_3, MoO_3	0.90:0.10:2	VCl_3	N/A	V_3O_5[a], V_2O_3[a]
VO_2, V_2O_3, MoO_3	0.80:0.20:2	VCl_3	N/A	MoO_2[a]
VO_2, V_2O_3, MoO_3	0.70:0.30:2	VCl_3	0.361(9)[a]	N/A
VO_2, V_2O_3, MoO_3	0.95:0.05:2	$MoCl_3$	0.051(6)[a]	N/A
VO_2, V_2O_3, MoO_3	0.90:0.10:2	$MoCl_3$	0.103(6)[a]	N/A
VO_2, V_2O_3, MoO_3	0.80:0.20:2	$MoCl_3$	0.209(7)[a]	V_4O_7[a]
VO_2, V_2O_3, MoO_3	0.70:0.30:2	$MoCl_3$	0.319(9)[a]	N/A
V_2O_3, MoO_3, MoO_2	0.60:0.40:2	$MoCl_3$	0.438(11)[a]	VOCl[a], V_2O_3[a]
V_2O_3, MoO_3, MoO_2	0.45:0.55:2	$MoCl_3$	0.545(13)[a]	V_2O_3[a]
V_2O_3, MoO_3, MoO_2	0.40:0.60:2	$MoCl_3$	0.598(14)[a]	Mo_4O_{11}[ab]
$V_{0.95}Mo_{0.05}O_2$	0.95:0.05:2	$TeCl_4$	0.052(6)[b]	N/A
$V_{0.90}Mo_{0.10}O_2$	0.90:0.10:2	$TeCl_4$	0.102(6)[b]	N/A
$V_{0.80}Mo_{0.20}O_2$	0.80:0.20:2	$TeCl_4$	0.218(8)[b]	N/A
$V_{0.70}Mo_{0.30}O_2$	0.70:0.30:2	$TeCl_4$	0.297(9)[b]	N/A
$V_{0.60}Mo_{0.40}O_2$	0.60:0.40:2	$TeCl_4$	0.394(10)[b]	N/A
$V_{0.45}Mo_{0.55}O_2$	0.45:0.55:2	$TeCl_4$	0.55(1)[b]	N/A
$V_{0.40}Mo_{0.60}O_2$	0.40:0.60:2	$TeCl_4$	0.60(1)[b]	Mo_4O_{11}[b]

[a]Compositions are taken from fitting PXRD lattice parameters to the known trend. Superscripts denote the end of the tube in which the product formed: [a]hot zone [b]cold zone.

single crystals of molybdenum doped VO_2 of the formula $V_{1-x}Mo_xO_2$ with molybdenum content up to $x = 0.60$.

EXPERIMENTAL SECTION

General Synthesis Method. Synthesis of $V_{1-x}Mo_xO_2$ was achieved using the chemical vapor transport (CVT) method. The varied parameters were primarily: reagent choice, input stoichiometry, and transport agent. The temperature gradient is the same for all reactions reported here: the dwell time was 6 days, the hot zone was 950 °C (9 h ramp on heating, 8 h ramp on cooling), and the cold zone was 850 °C (10 h ramp on heating, 9 h ramp on cooling).

The following reagents were used: VO_2 (Materion, 99.5%), V_2O_3 (Alfa Aesar, 99.7%), MoO_3 (Alfa Aesar, 99.95%), and MoO_2. MoO_2 was obtained through the reduction of MoO_3 by passing 5% H_2 gas in Ar over the MoO_3 for 24 h at 565 °C and verified using powder X-ray diffraction (PXRD). A total of 0.3 to 0.6 g of reagents were used. Transport agents used were VCl_3 (Alfa Aesar, 99%), $MoCl_3$(Alfa Aesar, 99.5%), and $TeCl_4$ (Alfa Aesar, 99.9%). For each reaction, samples were sealed in evacuated fused quartz ampules, with a 1 cm diameter, ~23 cm length and an equivalent mass of transport agent (0.15 mg) was used. All experiments were performed in the same furnace (a Lindberg Blue M three-zone tube furnace).

Optimized Synthesis Method. The various growth methods attempted are reported in the Results section below and tabulated in Table 1. On the basis of the results reported below, the optimized synthesis of large single crystal samples of $V_{1-x}Mo_xO_2$ for $0 \leq x \leq 0.60$ requires a two-part CVT synthesis with the first step used to synthesize phase-pure $V_{1-x}Mo_xO_2$ and the second step used for crystal growth. For the first step, the CVT-style setup was the only way found to prevent the formation of higher Mo-containing oxides in this step. The second step requires phase-pure $V_{1-x}Mo_xO_2$ as a precursor, otherwise molybdenum tellurate phases poison the reaction.

The first step uses $MoCl_3$ as a transport agent and starting materials chosen from VO_2, V_2O_3, MoO_3, and MoO_2 in order to give a V: Mo: O ratio to match the target composition. Given the oxidation state range available, multiple starting material compositions could be used (e.g., either 3:1 VO_2: MO_2 or 1:1:1 V_2O_3: VO_2: MoO_3 for $x = 0.25$), but the final composition of the main product was insensitive to this choice for this step.

The resulting products are a few, small single crystals of $V_{1-x}Mo_xO_2$ in the cold zone of the tube and a large amount of a black polycrystalline powder of phase-pure $V_{1-x}Mo_xO_2$ in the hot zone of the tube. Both the resulting single crystal and polycrystalline products have molybdenum compositions in close agreement to the initial input value.

To obtain larger single crystals, the phase pure polycrystalline samples from the hot zone were ground into a fine powder and placed into new evacuated ampules, this time using $TeCl_4$ as the transport agent, and heated using the same standardized heating schedule reported above. This second CVT synthesis resulted in the formation of single crystals of $V_{1-x}Mo_xO_2$, with x near that of the input value, in the cold zone. These crystals were large (5 mm × 0.5 mm × 0.5 mm), rod-shaped single crystals that, like the polycrystalline samples, were black in color with a slight bluish or purplish metallic cast.

Characterization. The room temperature PXRD scans were obtained using a Bruker D2 Phaser, Cu Kα radiation with structural models from GSAS and EXPGUI being used to fit the data.[14,15] The resulting lattice parameters were the primary method for determining composition. The compositions were verified against two other metrics on a subset of samples. (1) The V:Mo occupancy ratio was modeled using single crystal X-ray diffraction (SXRD) and (2) through inductively coupled plasma optical emission spectroscopy (ICP-OES) experiments. Additionally, sample homogeneity was confirmed using scanning electron microscopy (SEM) energy dispersive X-ray spectroscopy (EDS) analysis to obtain maps of the surface of several single crystals in the dopant range.

Single crystal diffraction data was collected using a Siemens diffractometer equipped with a Bruker APEX-II CCD and a monochromated Mo Kα producing sealed source and a Rigaku

https://dx.doi.org/10.1021/acs.cgd.9b01296
Cryst. Growth Des. 2020, 20, 3635−3640

XtaLAB Synergy R, DW system, equipped with HyPix detector. Structural models of the single crystal diffraction data were created and refined using SHELX and WINGX.[16,17] SEM-EDS data was collected using a Jeol 7000 FE SEM at an energy of 20.0 kV.

A PerkinElmer Optima 8300 ICP-OES with axial viewing was used for composition analysis. A calibration curve was developed using a multielement standard (Quality Control Standard 19, VWR, lot no. P2-MEB677343), the wavelengths used were Mo(II) 202.031 and V(II) 290.880 nm. The calibration curve was fit with a line forced through zero with all an R^2 value greater than 0.999 and all data was recorded in triplicate. No emission from other elements in the multielement standard overlap with the analyte peaks. All samples were delivered at 1.5 mL min^{-1} with a plasma flow of 15 L min^{-1}, auxiliary flow of 0.2 L min^{-1}, nebulizer flow of 0.55 L min^{-1}, and power of 1300 W.

RESULTS AND DISCUSSION

The first step to obtaining an optimized synthesis of $V_{1-x}Mo_xO_2$ single crystals was to determine an appropriate transport agent and temperature gradient for CVT. Because various vanadium oxides have previously been grown using a CVT synthesis with $TeCl_4$ as a transport agent and with a temperature gradient between 850 and 950 °C, this was chosen as the starting point for the synthesis.[18] Before proceeding with doping experiments, large (7 mm × 0.8 mm × 0.8 mm) single crystals of undoped VO_2, gray with a metallic sheen, were grown confirming this temperature schedule as a valid starting point for the synthesis.

Optimization by Reagent Choice. To obtain single crystals of molybdenum doped VO_2, it is necessary to determine an appropriate V: Mo: O ratio, as disproportionation may occur. This was done by selecting the molybdenum composition at which a 1:1 ratio of V^{3+} to V^{4+}, would balance with the 6+ oxidation state of the molybdenum in MoO_3 to give an overall 4+ oxidation state on the metal atom. This composition, $V_{0.8}Mo_{0.2}O_2$, was then synthesized using MoO_3 as the molybdenum source and then varying the amount of the V_2O_3 and VO_2 starting materials to obtain V^{3+}: V^{4+} ratios between 1:0 and 0:1, PXRD of the resulting phases are shown in Figure 1. Of these reactions, the fewest extraneous phases were found in the 1:1, V^{3+}: V^{4+}, sample. Therefore, a 1:1 ratio of V_2O_3: MoO_3 (i.e., 2:1 V^{3+}: Mo^{6+}) was used to maintain an overall 4+ oxidation state for the synthesis of $V_{1-x}Mo_xO_2$ with $0.05 \leq x \leq 0.33$.

For the above reactions, the hot zone of the tube contained nearly phase pure polycrystalline $V_{1-x}Mo_xO_2$, but there were very few single crystals obtained in the cold zone. Analysis of these crystals by single-crystal X-ray diffraction (SXRD) determined them to be $TeMo_5O_{16}$. Since tellurium from the transport agent was removed from the gas phase to form this side product, the reaction resulted in no transport of VO_2, leaving polycrystalline $V_{1-x}Mo_xO_2$, with an irreproducible molybdenum content remaining in the hot zone. This lack of transport also indicates that this unwanted reaction likely took place between the $TeCl_4$ transport agent and the MoO_3 starting material early in the reaction, possibly even before the furnace reached full temperature due to the high vapor pressure of MoO_3.

With the high vapor pressure of MoO_3 appearing to cause a reaction with the $TeCl_4$ transport agent, MoO_2 was chosen as an alternate molybdenum source to bypass the molybdenum tellurate byproduct. This CVT synthesis with only VO_2 and MoO_2 starting materials was successful in avoiding the molybdenum tellurate side product and lead to large single crystals of $V_{1-x}Mo_xO_2$. However, the output molybdenum composition was roughly half that of the input composition for all samples with excess MoO_2 crystals in the hot zone of the tube (Table 1).

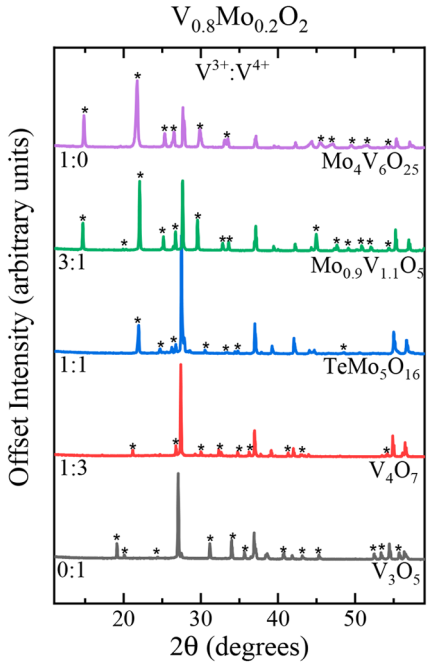

Figure 1. Oxygen content for $V_{0.8}Mo_{0.2}O_2$ was varied by changing the ratio of V^{3+} to V^{4+}. The most phase pure product was obtained for a 1:1 ratio indicating that the oxidation state of the metal needed to be balanced as an overall 4+ oxidation state. Byproducts for each synthesis are labeled below the corresponding diffraction pattern with the diffraction peaks for that byproduct being denoted by an asterisk.

Optimization by Transport Agent Choice. When using $TeCl_4$ as the transport, the use of both MoO_3 and MoO_2 as Mo sources had drawbacks that precluded the formation of large crystals with the desired molybdenum content. To avoid the formation of $TeMo_5O_{16}$ while maintaining control over the molybdenum content, two alternative transport agents, VCl_3 and $MoCl_3$, were tested using MoO_3 as the molybdenum source. These transport agents were selected as candidates because they each decompose into one or more gaseous product upon heating and only introduce chlorine as an additional element to the synthesis. Transport using VCl_3 failed to produce phase pure products; however, transport using $MoCl_3$ resulted in phase pure black phase-pure polycrystalline $V_{1-x}Mo_xO_2$ in the hot zone and very few, small (0.10 mm × 0.04 mm × 0.04 mm) single crystals of $V_{1-x}Mo_xO_2$ with $0 \leq x \leq 0.33$ obtained in the cold zone. These products were characterized using PXRD and SXRD (Table 1).

When attempting to obtain compositions of $V_{1-x}Mo_xO_2$ where $x > 0.33$ using only MoO_3 as the molybdenum source, the synthesis resulted in impure samples of lower compositions of $V_{1-x}Mo_xO_2$ with lower molybdenum concentration than the input composition as well as various vanadium and molybdenum Magnéli phases due to the oxygen content no longer being balanced to provide a 1:2 metal: oxygen ratio. Therefore, to exceed the $x = 0.33$ threshold, MoO_2 must be used to balance the oxygen content. By introducing MoO_2 as an additional reactant, polycrystalline samples of $V_{1-x}Mo_xO_2$ with $0 \leq x \leq 0.60$ were obtained (Table 1). Attempts to obtain

https://dx.doi.org/10.1021/acs.cgd.9b01296
Cryst. Growth Des. 2020, 20, 3635−3640

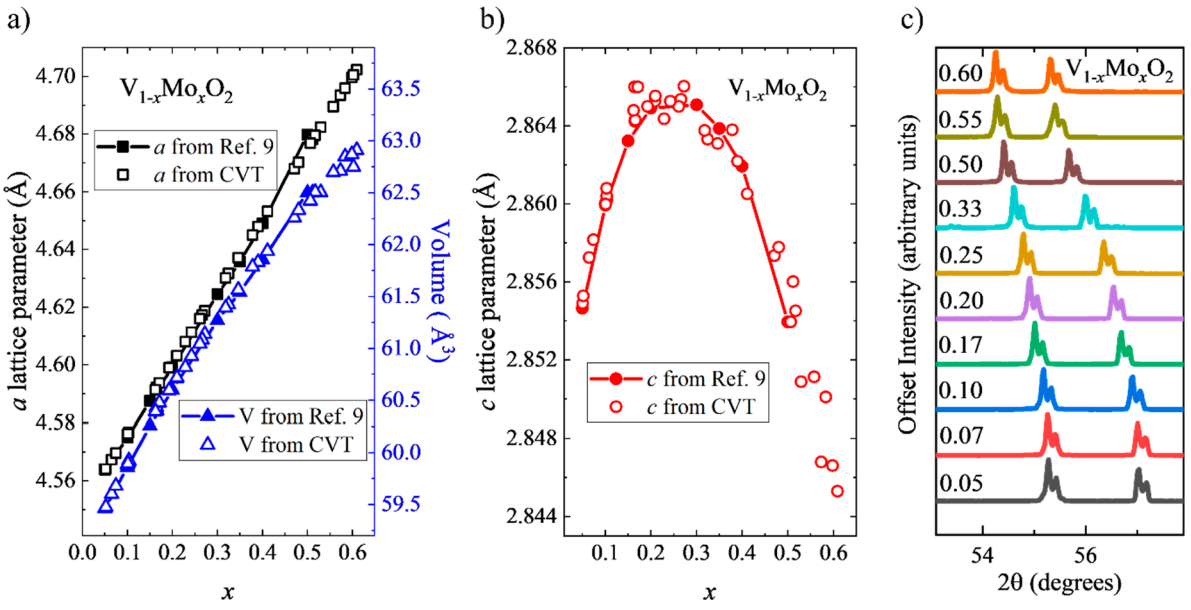

Figure 2. (a) Composition for the CVT growths were obtained by comparing known *a* lattice parameters to the a lattice parameters obtained by GSAS refinements. Once the composition was determined using the *a* lattice parameter, plots of the composition versus volume and (b) composition versus *c* lattice parameter were obtained in order to confirm that the obtained values matched well with the known trend. Error bars for both panels a and b are smaller than the points. (c) Plots for the range of dopant products show how the diffraction peaks change as a function of approximate dopant percentage.

$V_{1-x}Mo_xO_2$ with $x > 0.60$ have all failed due to the formation of pure MoO_2 and various molybdenum Magnéli phases. Since Mo^{4+} and V^{4+} are both found in products and in combination with the $Mo^{5,6+}$ species, this points to the possibility of a miscibility gap in this composition regime. However, it is also possible that by exerting even more reducing conditions that the composition range may be extended.

Final Optimization. While $MoCl_3$ provides good chemical control, the crystal size is only suitable for single crystal X-ray diffraction and not electronic transport or diffuse scattering measurements. Conversely, reactions using MoO_2 and $TeCl_4$ as the transport agent can provide larger single crystals, compositional control is lost. So, to average out the activity of the two metals while obtaining larger single crystals, we elected to use ground polycrystalline $V_{1-x}Mo_xO_2$ samples from the $MoCl_3$ growth attempts as a starting reagent in a second CVT reaction, but with $TeCl_4$ as the transport agent. This resulted in large (5 mm × 0.5 mm × 0.5 mm), rod-shaped single crystals of $V_{1-x}Mo_xO_2$ with output molybdenum compositions comparable to the input (Table 1) and no Mo−Te−O phases.

Finally, synthesis of $V_{1-x}Mo_xO_2$ without $MoCl_3$ was attempted as a way to more easily obtain $V_{1-x}Mo_xO_2$ powders, that is, using a standard solid-state reaction. For higher Mo content, this is unsuccessful. Apparently, the atmosphere of $MoCl_2$ and $MoCl_4$ gas from the decomposition of $MoCl_3$ is necessary to avoid the formation of molybdenum Magnéli phases, especially for higher molybdenum compositions. It is possible that in this case, the formation of higher molybdenum oxide phases is driven by molybdenum oxide vapors that form in the sealed ampule, and that the volatile molybdenum chlorides suppress their formation.

Compositional Determination. The concentration of molybdenum in the resulting $V_{1-x}Mo_xO_2$ samples was determined by comparing the PXRD lattice parameters against Holman et al. as a reference, as the *a* lattice parameter was shown to increase linearly with molybdenum composition.[9] Using this linear trend, the compositions of these $V_{1-x}Mo_xO_2$ samples were calculated and plotted (Figure 2a and b), which shows the close agreement with the previous report. Note that the compositions shown in the plot are tetragonal at room temperature. Figure 2c shows that the Bragg reflections shift smoothly but not monotonically with composition.

To verify the compositions determined using PXRD, ICP-OES was used as an external calibrant. The results are shown in Table 2. It can be seen the values are usually within about $\Delta x = 0.01$ on an absolute scale. Results from SXRD refinement occupancy models are also included for most of these cases. These values are less precise, as expected, but are usually within one std. of the PXRD and ICP-OES values. The crystallographic information files were deposited in the Inorganic Crystal Structure Database (ICSD): CSD 1990781−1990785 for x = 0.08, 0.11, 0.19, 0.45, and 0.54, respectively (referenced using ICP-OES values). Note that the single crystal structural solutions assumed a rutile crystal structure. In actuality, this is the long-range structure for all of the materials studied, but in many cases there are diffuse peaks that indicate complex short-range ordering. Characterization of the diffuse scattering is an ongoing endeavor.[19,20]

Table 2. $V_{1-x}Mo_xO_2$, Determination of x Using Three Separate Methods on the Same Batch[a]

input	SXRD	PXRD	ICP-OES
0.05	0.076(15)	0.074(6)	0.078(3)
0.10	0.082(8)	0.095(6)	0.1062(12)
0.40	0.20(2)	0.187(7)	0.1881(17)
0.30		0.319(9)	0.333(2)
0.40	0.412(12)	0.438(11)	0.4526(1)
0.55	0.52(3)	0.55(1)	0.53608(3)

[a]Note that similar input composition can lead to different final compositions depending on the reaction conditions (Table 1).

https://dx.doi.org/10.1021/acs.cgd.9b01296
Cryst. Growth Des. 2020, 20, 3635−3640

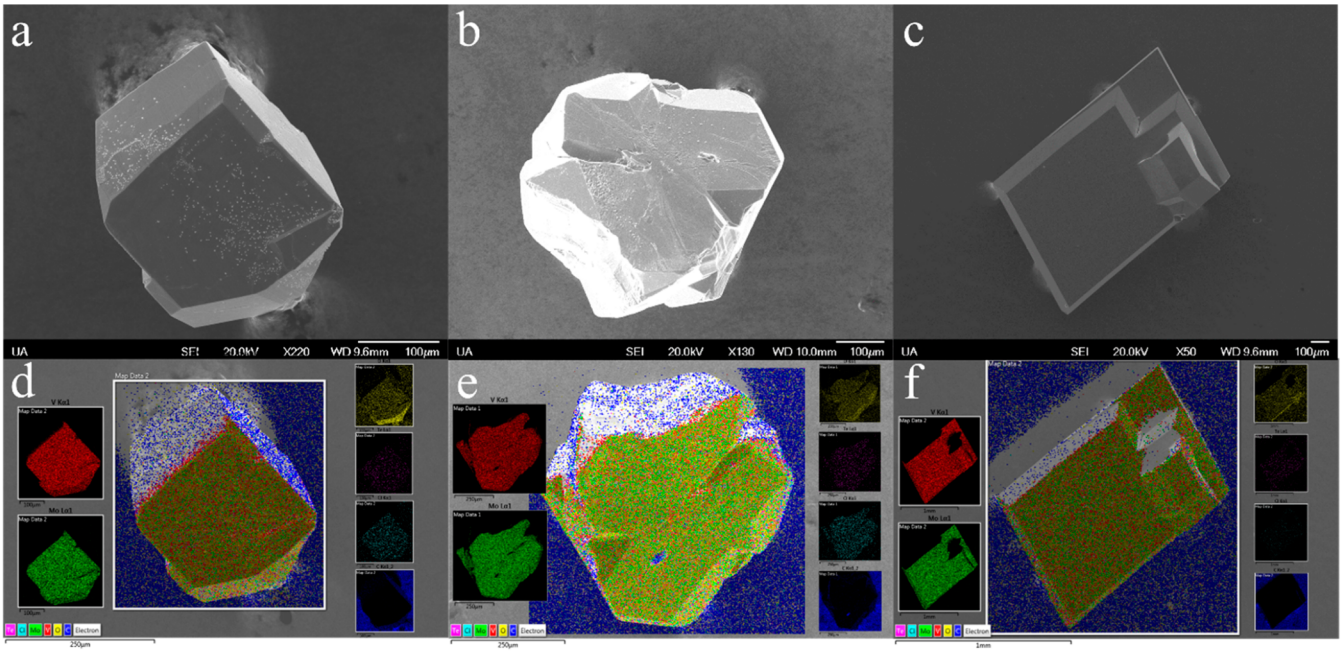

Figure 3. SEM images of $V_{1-x}Mo_xO_2$ for x = (a) 0.10, (b) 0.33, and (c) 0.40. EDS maps for the incorporated elements are below the SEM images in panels d–f. In the EDS maps, vanadium is red, molybdenum is green, oxygen is yellow, tellurium is purple, chlorine is cyan, and carbon is blue.

The chemical homogeneity of the crystals is observed in the SEM (Figure 3). The crystals are generally well-formed, and there is no appreciable difference in composition between crystals in a batch or on different points in the same crystal. Te and Cl were included in the spectral analysis, but typically represented less than 1% of present species by atomic fraction. Further images can be found in the Supporting Information.

CONCLUSION

The synthesis of $V_{1-x}Mo_xO_2$ has been optimized to obtain large single crystals through the use of a two-step CVT synthesis. This two-step synthesis was necessary to avoid unwanted side reactions with the transport agent while still being able to obtain large single crystals suitable for physical property measurements and diffuse scattering experiments. Additionally, by using an atmosphere of $MoCl_2$ and $MoCl_4$ to suppress the formation of volatile molybdenum oxide phases, both single crystal and polycrystalline samples of $V_{1-x}Mo_xO_2$ can be obtained with higher molybdenum concentrations than what was possible through previous synthetic methods. Through further optimization of this synthesis, single crystals for the entire VO_2–MoO_2 dopant range might be possible. This type of two-step synthesis could prove beneficial in other crystal systems where CVT synthesis has previously failed because of the reaction between starting materials and otherwise optimal transport agents.

ASSOCIATED CONTENT

Supporting Information

The Supporting Information is available free of charge at https://pubs.acs.org/doi/10.1021/acs.cgd.9b01296.

Optical images of crystals, additional SEM micrographs of crystals, and additional PXRD scans of polycrystalline $V_{1-x}Mo_xO_2$ prepared from the synthesized crystals (PDF)

Accession Codes

CCDC 1990781–1990785 contain the supplementary crystallographic data for this paper. These data can be obtained free of charge via www.ccdc.cam.ac.uk/data_request/cif, or by emailing data_request@ccdc.cam.ac.uk, or by contacting The Cambridge Crystallographic Data Centre, 12 Union Road, Cambridge CB2 1EZ, UK; fax: +44 1223 336033.

AUTHOR INFORMATION

Corresponding Author

Jared M. Allred – *Department of Chemistry and Biochemistry, The University of Alabama, Tuscaloosa, Alabama 35487, United States;* orcid.org/0000-0002-5953-300X; Email: jmallred@ua.edu

Authors

Matthew A. Davenport – *Department of Chemistry and Biochemistry, The University of Alabama, Tuscaloosa, Alabama 35487, United States*

Matthew P. Confer – *Department of Chemistry and Biochemistry, The University of Alabama, Tuscaloosa, Alabama 35487, United States; Department of Chemical and Biological Engineering, University of Alabama, Tuscaloosa, Alabama 35487, United States;* orcid.org/0000-0002-0856-3583

Tyra C. Douglas – *Department of Chemistry and Biochemistry, The University of Alabama, Tuscaloosa, Alabama 35487, United States;* orcid.org/0000-0002-1142-6846

Top B. Rawot Chhetri – *Department of Chemistry and Biochemistry, The University of Alabama, Tuscaloosa, Alabama 35487, United States*

Complete contact information is available at: https://pubs.acs.org/10.1021/acs.cgd.9b01296

Notes

The authors declare no competing financial interest.

https://dx.doi.org/10.1021/acs.cgd.9b01296
Cryst. Growth Des. 2020, 20, 3635–3640

■ ACKNOWLEDGMENTS

The work was supported by the U.S. Department of Energy, Office of Basic Energy Sciences under award DE-SC0018174. The authors thank NSF CHE MRI 1828078 and UA for the purchase of the single crystal X-ray diffraction instrument used for some of the structural solutions. The authors also gratefully acknowledge the University of Alabama College of Engineering and College of Arts and Sciences shared analytical facility for providing use of the ICP-OES.

■ REFERENCES

(1) Morin, F. J. Oxides Which Show a Metal-to-Insulator Transition at the Neel Temperature. *Phys. Rev. Lett.* **1959**, *3*, 34−36.
(2) Andersson, G.; Parck, C.; Ulfvarson, U.; Stenhagen, E.; Thorell, B. Studies on Vanadium Oxides. *Acta Chem. Scand.* **1956**, *10*, 623−628.
(3) Mott, N. F. Metal-Insulator Transition. *Rev. Mod. Phys.* **1968**, *40*, 677−683.
(4) Peierls, R. *More Surprises in Theoretical Physics*; Princeton University Press, 1991.
(5) Sakuma, R; Miyake, T; Aryasetiawan, F Quasiparticle Band Structure of Vanadium Dioxide. *J. Phys.: Condens. Matter* **2009**, *21*, 064226.
(6) Budai, J. D.; Hong, J.; Manley, M. E.; Specht, E. D.; Li, C. W.; Tischler, J. Z.; Abernathy, D. L.; Said, A. H.; Leu, B. M.; Boatner, L. A.; McQueeney, R. J.; Delaire, O. Metallization of Vanadium Dioxide Driven by large Phonon Entropy. *Nature* **2014**, *515*, 535−539.
(7) Pouget, J. P.; Launois, H.; D'Haenens, J. P.; Merenda, P.; Rice, T. M. Electron Localization induced by uniaxial stress in pure VO_2. *Phys. Rev. Lett.* **1975**, *35*, 873.
(8) Tang, C.; Georgopoulos, P.; Fine, M. E.; Cohen, J. B.; Nygren, M.; Knapp, G. S.; Aldred, A. Local Atomic and Electronic Arrangements in $W_xV_{1-x}O_2$. *Phys. Rev. B: Condens. Matter Mater. Phys.* **1985**, *31*, 1000.
(9) Holman, K. L.; McQueen, T. M.; Williams, A. J.; Klimczuk, T.; Stephens, P. W.; Zandbergen, H. W.; Xu, Q.; Ronning, F.; Cava, R. J. Insulator to Correlated Metal Transition in $V_{1-x}Mo_xO_2$. *Phys. Rev. B: Condens. Matter Mater. Phys.* **2009**, *79*, 245114.
(10) Béteille, F.; Morineau, R.; Livage, J.; Nagano, M. Switching properties of $V_{1-x}Ti_xO_2$ thin films deposited from alkoxides. *Mater. Res. Bull.* **1997**, *32*, 1109−1117.
(11) Pouget, J. P.; Launois, H.; Rice, T. M.; Dernier, P.; Gossard, A.; Villeneuve, G.; Hagenmuller, P. Dimerization of a linear heisenberg chain in insulating phases of $V_{1-x}Cr_xO_2$. *Phys. Rev. B* **1974**, *10*, 1801.
(12) Kong, T.; Masters, M. W.; Bud'ko, S. L.; Canfield, P. C. Physical properties of $V_{1-x}Ti_xO_2$ ($0 < x < 0.187$) single crystals. *APL Mater.* **2015**, *3*, 041502.
(13) Ghedira, M.; Vincent, H.; Marezio, M.; Launay, J. C. Structural aspects of metal-insulatro transitions in $V_{0.985}AL_{0.015}O_2$. *J. Solid State Chem.* **1977**, *22*, 423−438.
(14) Toby, B. H. Expgui, a graphical user interface of gsas. *J. Appl. Crystallogr.* **2001**, *34*, 210−213.
(15) Larson, A. C.; Dreele, R. B. V. General structure analysis system (gsas). *Los Alamos National Laboratory Report* **2000**, 86−748.
(16) Sheldrick, G. M. A short history of SHELX. *Acta Crystallogr., Sect. A: Found. Crystallogr.* **2008**, *64*, 112−122.
(17) Farrugia, L. J. WinGX Suite for Small-Molecule Single-Crystal Crystallography. *J. Appl. Crystallogr.* **1999**, *32*, 837−838.
(18) Allred, J. M.; Cava, R. J. Crystal structures of the high temperature forms of V_8O_{15} and V_9O_{17} and structural trends in the V_nO_{2n-1} Magnéli series. *J. Solid State Chem.* **2013**, *198*, 10−17.
(19) Davenport, M. A.; Krogstad, M. J.; Whitt, L. M.; Hu, h.; Douglas, T. C.; Ni, N.; Rosenkranz, S.; Osborn, R.; Allred, J. M., Fragile 3D Order in $V_{1-x}Mo_xO_2$. *arXiv (Strongly Correlated Electrons)*, 2019, 1909.12704. https://arxiv.org/abs/1909.12704.
(20) Davenport, M. A.; Allred, J. M., A crystallographic approach to the short-range ordering problem in $V_{1-x}Mo_xO_2$ ($0.50 \leq x \leq 0.60$). Unpublished work, 2020.

https://dx.doi.org/10.1021/acs.cgd.9b01296
Cryst. Growth Des. 2020, 20, 3635−3640